J Eng Math (2014) 86:9–29
DOI 10.1007/s10665-013-9651-8

Impact of interfacial slip on the stability of liquid two-layer polymer films

Sebastian Jachalski · Dirk Peschka · Andreas Münch · Barbara Wagner

Received: 4 November 2012 / Accepted: 6 May 2013 / Published online: 16 November 2013

Abstract In this work we derive systems of coupled thin-film equations for immiscible liquid polymer layers on a solid substrate. We take into account slip between liquids and solids and also slip between both liquids. On the scale of tens of nanometres, such two-layer systems are susceptible to instability and may rupture and dewet due to intermolecular forces. The stability of the two-layer system and its significant dependence on the order of magnitude of slip is investigated via these thin-film models. With weak slip at both the liquid–liquid and liquid–solid interfaces and polymer layers of comparable thickness, the dispersion relation typically shows two local maxima, one in the long-wave regime and the other at moderate wavenumbers. The former is associated with perturbations that mainly affect the gas–liquid interface and the latter with larger relative perturbation amplitudes at the liquid–liquid interface. Increasing the slip at the liquid–liquid interface generally favours the long-wave regime and can in fact revert the mode of the instability and thus significantly change the spinodal patterns. Moreover, the maxima shift to small wavenumbers for increasing slip.

Keywords Fluid dynamics · Interfacial slip · Thin-film models · Two-phase flow

1 Introduction

The stability of thin liquid films is of great interest in many technological applications involving lubricants and coatings. In particular, when the thickness of films is on the micro- to nanoscale, bulk and surface stresses compete with intermolecular forces and may lead to complex wetting or dewetting dynamics. Understanding and controlling this dynamics is fundamental in nanoscale design and functionalisation of surfaces for numerous applications ranging from optoelectronics to biotechnology. However, while stability, rupture and dewetting of liquid films on solid substrates have been investigated intensively experimentally and theoretically in recent decades, comparatively

S. Jachalski · D. Peschka
Weierstrass Institute for Applied Analysis and Stochastics, Mohrenstraße 39, 10117 Berlin, Germany

A. Münch (✉)
Mathematical Institute, University of Oxford, 24-29 St. Giles', Oxford OX1 3LB, UK
e-mail: muench@maths.ox.ac.uk

B. Wagner
Institute of Mathematics, Technische Universtät Berlin, Straße des 17. Juni 136, 10623 Berlin, Germany

fewer studies have been conducted on two-layer immiscible liquid films. Moreover, two-layer liquid films have a far richer dynamics and potentially more complex morphological structures even when both liquid layers are Newtonian. Here, apart from differences in the thickness and density of the two layers, additional parameters such as the ratio of the viscosities of both liquids and the ratio of the interfacial tension coefficients can play a dominant role in determining the morphological structure.

Some of these effects are explored in an early experimental and theoretical study on liquid–liquid dewetting in [1]. Two-layer systems were investigated using linear stability analysis as well as numerical simulations including rupture. This was carried out in the framework of lubrication theory by Pototsky et al. [2,3], Fisher and Golovin [4,5], Bandyopadhyay et al. [6,7] and Craster and Matar [8]. Also, stationary droplet solutions for liquid–liquid systems and their stability have been studied numerically for the coupled system of thin-film equations by Pototsky et al. [3]. Related studies of stratified thin films between parallel surfaces, where slip may also have to be taken into account, can be found in [9,10]. In a recent article, Thiele et al. [11] pointed out that liquid–liquid systems have a variational structure similar to that of systems for surfactants on thin films. Many more studies are found in a recent comprehensive review on both single- and two-layer systems by Craster and Matar [12], illustrating the extent of work in this field.

Interestingly, interfacial slip between immiscible, liquid polymer layers has not been taken into account in the framework of two-layer thin-film models, even though the work by Lin [13] already suggested the possibility of interfacial slip, and a number of experimental studies have demonstrated clear evidence of slip at polymer–polymer interfaces. Most importantly, we mention here the coextrusion experiments by Zhao and Macosko [14] that exhibit slip, in particular between polystyrene (PS) and polymethylmethacrylate (PMMA) interfaces, as well as more recent measurements by Zeng et al. [15], and in liquid two-layer systems of PS dewetting from PMMA by Lin et al. [16]. On the other hand, the intensely investigated slip phenomenon for thin polymer films on solid substrates, for example as occurs when a polymer film dewets a hydrophobically coated substrate, has often been described by a Navier-slip condition, relating the lateral velocity along the substrate to the shear rate $u = b\,u_z$, with the extrapolation length b being a measure of the slip length. In fact, b is an apparent slip length that reflects the underlying microscopic mechanism. A well-known example is the case of polymer melts dewetting from a monolayer of polymer chains grafted on a substrate, for which Brochard-Wyart and de Gennes [17] showed that b could be derived from microscopic consideration as a coil-stretch transition into a disentangled state with much lower Rouse friction, and hence viscosity, within a very thin layer near the substrate. Other mechanisms corresponding to different liquid–solid systems exhibiting apparent slip are described in [18] and the review by Lauga et al. [19].

While these results are of fundamental importance, they have also led to the derivation of new thin-film models, in particular for dewetting polymer melts, that take into account apparent slip of various orders of magnitude. The investigations by Kargupta et al. [20] showed a strong dependence of the time scale of rupture and density of holes of the typically unstable polymer film on the slip length. In [21,22] it was shown that the dynamics and morphology of dewetting rims may even be controlled by slippage. Their models systematically explained experimental results on the shape of the rim that were previously attributed to viscoelastic effects [23,24] and, moreover, established a new experimental method for assessing slip in thin polymer films [25,26]. As a result of these studies, it was shown that the bulk of a dewetting thin film can be described as a Newtonian fluid as long as the chain length of the polymer remains below the entanglement length. However, the large slip is in fact a signature of the non-Newtonian flow properties of the liquid polymer.

Thin-film models for immiscible polymer layers taking into account the orders of magnitude of interfacial slip are the main topic of this study; such models make use of the theories and analysis of the microscopic mechanisms at the polymer–polymer interface under shearing motion. The derivation of apparent slip at polymer–polymer interfaces has been developed in works by Goveas and Fredrickson [27] and Adhikari and Goveas [28], extending earlier work by de Gennes, Brochard-Wyart and Ajdari [29–31] for unentangled polymer, entangled polymer, dilute polymer emulsions, and for cases when both liquid layers are Newtonian. In essence, the repulsive forces within a thin interfacial region of two immiscible polymer films introduce higher shear rates and, hence, an apparent velocity jump, leading to the concept of apparent slip.

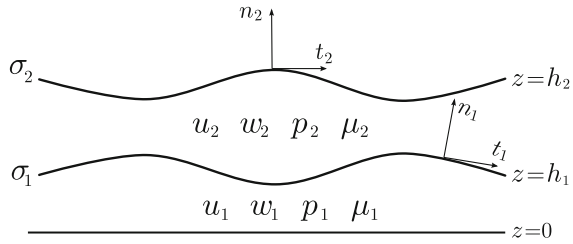

Fig. 1 Sketch of a two-layer system

As for single polymer layers on a solid substrate, dimension-reduced thin-film models allow for the systematic analysis and efficient numerical simulation of the morphological evolution. The focus of this article is to describe and analyse the possible impact of slip on the stability properties of the interfaces of a two-layer system. We thus derive in Sect. 3 two thin-film models as asymptotic limits from the underlying fluid-dynamical model for the two-layer system introduced in Sect. 2. These thin-film models take account of different orders of magnitude of slip. The first model includes weak-slip conditions at the liquid–solid boundary as well as at the liquid–liquid interface. The second thin-film model allows for strong slip at both liquid–solid and liquid–liquid interfaces, i.e. orders of magnitude larger than weak slip. The focus of Sect. 4 will be to derive the dispersion relations and the dominant spinodal wavelength and to determine the mode of the perturbation of the two interfaces, such as sinuous or varicose. This is obtained via a linear stability analysis about flat constant interfaces. While these are fairly standard and straightforward calculations, the fact that the base states are constant allows the stability analysis for the underlying Stokes problem to be carried out easily. We thus are able to make direct comparisons with results of the thin-film models in their respective asymptotic limits. This in turn will delimit the range of validity of the new thin-film models as the slip lengths are varied, which will also be of importance for the further analysis of these models.

We further point out that, although there are a number of potential combinations of slip conditions for different orders of magnitude at the solid substrate and the liquid–liquid interface and hence further asymptotic limits, we analyse here only the two thin-film models mentioned earlier since they show most clearly the significant impact of interfacial slip on the stability behaviour of the liquid–liquid system. In particular, we describe the case where strong-slip conditions are imposed at both interfaces, with a strong coupling of the dynamics of the interfaces. Most notably, our results show that the impact of slip may not only change the value of the dominant wavelength but may even reverse the type of the most unstable mode. This observation may have important implications in interpreting the stability properties in an experimental setting.

2 Formulation

The basic situation where two liquid layers are deposited on a solid substrate is depicted in Fig. 1. Coordinates are introduced with the x-axis pointing in the lateral direction, along the flat solid substrate, and the z-axis pointing normal to it. The solid–liquid interface is located at $z = 0$, and the liquid–liquid and liquid–gas interfaces at $z = h_1(x, t)$ and $z = h_2(x, t)$, respectively, where t denotes time. The variables u_n, w_n and p_n denote the lateral and vertical velocity components and the pressure, respectively, in the nth layer, with $n = 1, 2$. The viscosity is denoted by $\mu_n, n = 1, 2$, for the two layers. Surface tensions for the liquid–liquid and liquid–gas interface are given by σ_1 and σ_2, respectively.

In both layers, we have the Navier–Stokes and mass conservation equations for incompressible Newtonian liquids:

$$\rho \frac{\mathrm{d}u_n}{\mathrm{d}t} = -\partial_x p_n + \mu_n \left(\partial_{xx} u_n + \partial_{zz} u_n\right), \tag{2.1a}$$

$$\rho \frac{\mathrm{d}w_n}{\mathrm{d}t} = -\partial_z p_n + \mu_n \left(\partial_{xx} w_n + \partial_{zz} w_n\right), \tag{2.1b}$$

$$\partial_x u_n + \partial_z w_n = 0, \tag{2.1c}$$

where $\mathrm{d}/\mathrm{d}t$ is the material derivate in each layer, $\mathrm{d}/\mathrm{d}t = \partial_t + u_n\partial_x + w_n\partial_z$, and $n = 1, 2$. For simplicity, we assume that both layers have the same density ρ. At the substrate $z = 0$, we impose the Navier-slip condition with slip length b and the impermeability condition

$$u_1 = b\,\partial_z u_1, \quad w_1 = 0. \tag{2.2a}$$

The free surface $z = h_2(x, t)$ evolves with the flow according to the kinematic condition,

$$(0, \partial_t h_2) \cdot \boldsymbol{n}_2 = (u_2, w_2) \cdot \boldsymbol{n}_2, \tag{2.2b}$$

and the tangential and normal stress condition, which are, respectively,

$$\boldsymbol{n}_2 \cdot \big(\Pi_2 + \phi'(h)I\big) \cdot \boldsymbol{t}_2 = 0, \tag{2.2c}$$

$$\boldsymbol{n}_2 \cdot \big(\Pi_2 + \phi'(h)I\big) \cdot \boldsymbol{n}_2 = \sigma_2\kappa_2. \tag{2.2d}$$

The term with $\phi(h)$ represents the effect of intermolecular forces, and its exact form will be given in (2.7). Similarly, at the liquid–liquid interface $z = h_1(x, t)$, we have the kinematic condition, tangential and normal stress conditions, and the impermeability and slip conditions with slip length b_1, which are, respectively,

$$(0, \partial_t h_1) \cdot \boldsymbol{n}_1 = (u_1, w_1) \cdot \boldsymbol{n}_1, \tag{2.3a}$$

$$\boldsymbol{n}_1 \cdot \big(\Pi_1 - \Pi_2 - \phi'(h)I\big) \cdot \boldsymbol{t}_1 = 0, \tag{2.3b}$$

$$\boldsymbol{n}_1 \cdot \big(\Pi_1 - \Pi_2 - \phi'(h)I\big) \cdot \boldsymbol{n}_1 = \sigma_1\kappa_1, \tag{2.3c}$$

$$(u_2 - u_1, w_2 - w_1) \cdot \boldsymbol{n}_1 = 0, \tag{2.3d}$$

$$(u_2 - u_1, w_2 - w_1) \cdot \boldsymbol{t}_1 = b_1 \left(\frac{1}{\mu_1} + \frac{1}{\mu_2}\right) \boldsymbol{n}_1 \cdot \Pi_2 \cdot \boldsymbol{t}_1. \tag{2.3e}$$

Here we denote the thickness of the top layer by

$$h(x, t) = h_2(x, t) - h_1(x, t), \tag{2.4}$$

the stress and strain tensors in the nth layer $n = 1, 2$ by

$$\Pi_n = -p_n I + \mu_2\dot{\gamma}_n, \quad \text{where} \quad \gamma_n = \partial_\ell u_{nk} + \partial_k u_{n\ell}, \tag{2.5}$$

and the unit tangential and normal vectors and curvature of the two interfaces $n = 1, 2$ by

$$\boldsymbol{n}_n = \frac{(-\partial_x h_n, 1)}{\sqrt{1 + (\partial_x h_n)^2}}, \quad \boldsymbol{t}_n = \frac{(1, \partial_x h_n)}{\sqrt{1 + (\partial_x h_n)^2}}, \quad \kappa_n = \nabla \cdot \boldsymbol{n}_n. \tag{2.6}$$

We focus on a situation where the contributions to the surface forces from the interaction with the solid substrate can be neglected, but the interaction with the bottom layer is relevant and can drive spinodal dewetting. Since these interactions decrease with the thickness of the bottom and top layers, respectively, this can be achieved, for example, by considering thin enough top layers and only moderately thin bottom layers. For the intermolecular potential we use the form

$$\phi(h) = \frac{8}{3}\phi_* \left[\frac{1}{8}\left(\frac{h_*}{h}\right)^8 - \frac{1}{2}\left(\frac{h_*}{h}\right)^2\right]. \tag{2.7}$$

This potential represents a contribution to the energy of a thin layer of thickness h. Variation of h_1 and h_2 changes this contribution by $-\phi'(h)\delta h_1$ and $\phi'(h)\delta h_2$, respectively; thus, we have a contribution $\phi'(h)$ to the normal force resisting and enhancing these variations in (2.2d) and (2.3c), respectively. The h^{-2} term in (2.7) represents the disjoining pressure contribution from the van der Waals forces that drives the dewetting, while the h^{-8} term is relevant only at very small thicknesses and is stabilising. In fact, the potential has a minimum $\phi_* < 0$ at $h = h_*$. As a general remark, we note that while the long-range part arises from a Lennard–Jones potential [32], the form, and in particular the power (here 8), in the short-range part of the potential may vary depending on the type of short-range forces are considered. In the literature, the power 3 is also often used instead. Other choices, such as exponentially decaying interactions for the short-range forces, are given in [33] and are used for example in [3]. Detailed discussions of the body of work in this field can be found in a recent review by Bonn et al. [34].

For our more general considerations we have chosen the stabilising part of the potential more for convenience in order to produce a minimum for a particular thickness of the film.

2.1 Nondimensional problem

Let H denote the typical thickness of the upper layer, i.e. of $h_2 - h_1$, and let L, U and P be a characteristic lateral length, velocity and pressure scale. We introduce these scalings via

$$\begin{aligned} &x = L\tilde{x}, \quad z = H\tilde{z}, \qquad h_i = H\tilde{h}_i, \quad b = H\tilde{b}, \quad b_1 = H\tilde{b}_1, \\ &u_n = U\tilde{u}_n, \quad w_n = W\tilde{w}_n, \quad t = \tfrac{L}{U}\tilde{t}, \\ &p_i = P\tilde{p}_i, \quad \phi' = P\tilde{\phi}', \end{aligned} \tag{2.8}$$

and then drop '$\sim$'. A pressure scale is set by the derivative of the intermolecular potential. The choice

$$P = \frac{8}{3}\frac{\phi_*}{H} \tag{2.9}$$

results in a particularly simple form for ϕ',

$$\phi'(h) = \frac{1}{\varepsilon}\left[-\left(\frac{\varepsilon}{h}\right)^9 + \left(\frac{\varepsilon}{h}\right)^3\right], \qquad \text{where} \quad \varepsilon = \frac{h_*}{H}. \tag{2.10}$$

In what follows we denote

$$\varepsilon_\ell = \frac{H}{L}, \qquad \mathrm{Re} = \frac{\rho U H}{\mu_2}, \qquad \mu = \frac{\mu_1}{\mu_2}, \qquad \sigma = \frac{\sigma_1}{\sigma_2}, \qquad \alpha = \frac{PH}{\mu_2 U}. \tag{2.11}$$

For the equations in the bulk of the liquid layers, we obtain

$$\varepsilon_\ell\,\mathrm{Re}\,\frac{\mathrm{d}u_2}{\mathrm{d}t} = -\alpha\,\varepsilon_\ell\partial_x p_2 + \varepsilon_\ell^2\partial_{xx}u_2 + \partial_{zz}u_2, \tag{2.12a}$$

$$\varepsilon_\ell^2\,\mathrm{Re}\,\frac{\mathrm{d}w_2}{\mathrm{d}t} = -\alpha\,\partial_z p_2 + \varepsilon_\ell^3\partial_{xx}w_2 + \varepsilon_\ell\partial_{zz}w_2, \tag{2.12b}$$

$$0 = \partial_x u_2 + \partial_z w_2, \tag{2.12c}$$

$$\varepsilon_\ell\,\mathrm{Re}\,\frac{\mathrm{d}u_1}{\mathrm{d}t} = -\alpha\,\varepsilon_\ell\partial_x p_1 + \mu\left(\varepsilon_\ell^2\partial_{xx}u_1 + \partial_{zz}u_1\right), \tag{2.12d}$$

$$\varepsilon_\ell^2\,\mathrm{Re}\,\frac{\mathrm{d}w_1}{\mathrm{d}t} = -\alpha\,\partial_z p_1 + \mu\left(\varepsilon_\ell^3\partial_{xx}w_1 + \varepsilon_\ell\partial_{zz}w_1\right), \tag{2.12e}$$

$$0 = \partial_x u_1 + \partial_z w_1. \tag{2.12f}$$

At the free surface $z = h_2$ we get for the normal, tangential and kinematic condition, respectively

$$p_2 - \phi'(h) + \frac{\partial_{xx}h_2}{\left[1+\varepsilon_\ell^2\left(\partial_x h_2\right)^2\right]^{3/2}} = 2\frac{\varepsilon_\ell}{\alpha}\frac{\left[1-\varepsilon_\ell^2\left(\partial_x h_2\right)^2\right]\partial_z w_2 - \left[\partial_z u_2 + \varepsilon_\ell^2\partial_x w_2\right]\partial_x h_2}{1+\varepsilon_\ell^2\left(\partial_x h_2\right)^2}, \tag{2.12g}$$

$$\left[\partial_z u_2 + \varepsilon_\ell^2\partial_x w_2\right]\left[1-\varepsilon_\ell^2\left(\partial_x h_2\right)^2\right] - 4\varepsilon_\ell^2\partial_x u_2\partial_x h_2 = 0, \tag{2.12h}$$

$$\partial_t h_2 = w_2 - u_2\partial_x h_2. \tag{2.12i}$$

For the boundary condition at the free liquid–liquid interface $z = h_1$ we get for the normal, tangential and kinematic condition, respectively,

$$\begin{aligned} &p_1 - p_2 + \phi'(h) + \sigma\,\frac{\partial_{xx}h_1}{\left[1+\varepsilon_\ell^2\left(\partial_x h_1\right)^2\right]^{3/2}} \\ &\quad = 2\frac{\varepsilon_\ell}{\alpha}\frac{\left[1-\varepsilon_\ell^2\left(\partial_x h_1\right)^2\right]\partial_z\left(\mu w_1 - w_2\right) - \left[\partial_z\left(\mu u_1 - u_2\right) + \varepsilon_\ell^2\partial_z\left(\mu w_1 - w_2\right)\right]\partial_x h_1}{1+\varepsilon_\ell^2\left(\partial_x h_1\right)^2}, \end{aligned} \tag{2.12j}$$

$$\left[\partial_z\left(\mu u_1 - u_2\right) + \varepsilon_\ell^2\partial_x\left(\mu w_1 - w_2\right)\right]\left[1-\varepsilon_\ell^2\left(\partial_x h_1\right)^2\right] - 4\varepsilon_\ell^2\partial_x\left(\mu u_1 - u_2\right)\partial_x h_1 = 0, \tag{2.12k}$$

$$\partial_t h_1 = w_1 - u_1\partial_x h_2. \tag{2.12l}$$

The impermeability condition between the upper and lower liquid layers is given by

$$(w_2 - w_1) - (u_2 - u_1)\,\partial_x h_1 = 0. \tag{2.12m}$$

The slip condition at the liquid–liquid interface becomes

$$(u_2 - u_1) + \varepsilon_\ell^2\,(w_2 - w_1)\,\partial_x h_1 = b_1\,\frac{\mu+1}{\mu}\,\frac{\left[\partial_z u_2 + \varepsilon_\ell^2 \partial_x w_2\right]\left[1 - \varepsilon_\ell^2\,(\partial_x h_1)^2\right] - 4\varepsilon_\ell^2 \partial_x u_2 \partial_x h_1}{\sqrt{1 + \varepsilon_\ell^2\,(\partial_x h_1)^2}}, \tag{2.12n}$$

and the boundary conditions (impermeability and Navier-slip) at the substrate are

$$w_1 = 0, \quad u_1 = b\,\partial_z u_1. \tag{2.12o}$$

Using the balance in Eq. (2.12g) we fix the parameter L by setting

$$\frac{\sigma_2 H}{PL^2} = 1. \tag{2.13}$$

Together with (2.9), we then find

$$\varepsilon_\ell = \frac{H}{L} = \sqrt{\frac{8}{3}\frac{\phi_*}{\sigma_2}}. \tag{2.14}$$

Throughout this paper, we assume that $\varepsilon_\ell \ll 1$ and derive thin-film equations for the profiles h_2 and h_1 for various degrees of slip at the solid–liquid and liquid–liquid interfaces. Different magnitudes of slip lengths will require different choices for α in terms of the small parameter ε_ℓ. We will treat μ and σ as parameters of order one. For many systems, such as dewetting micro- and nanoscopic polymer films, inertia is negligibly small. Therefore, we will only cover the case $\mathrm{Re} = 0$ but remark that inertia can be kept easily for the strong-slip models in appropriate regimes of Re, analogous to one-layer models [21].

3 Thin-film models

3.1 Weak-slip model

In this section we assume that both slip lengths are $O(1)$. We will refer to the resulting thin-film model as the weak-slip model. Here, the flow is driven by the lateral pressure gradient $\partial_x p$ acting on the dominant viscous term $\partial_{zz} u_2$ in (2.12a). Thus we balance the two by letting

$$\alpha = \frac{1}{\varepsilon_\ell}, \tag{3.1}$$

which fixes the velocity scale and, thus, the capillary number in terms of ε_ℓ,

$$\mathrm{Ca} = \frac{\mu_2 U}{\sigma_2} = \varepsilon_\ell^3. \tag{3.2}$$

The corresponding leading-order problem in (2.12) can then be integrated and reduced to the system of partial differential equations for $h_2(x,t)$ and $h_1(x,t)$ using the kinematic conditions (2.12i) and (2.12l). The derivation is a straightforward variation of the case where there is no slip at both interfaces; see e.g. [2,8]. Here we find it more convenient to write the thin-film model as a system for $h_1(x,t)$ and $h(x,t) = h_2(x,t) - h_1(x,t)$. To do this, note that

$$\partial_t h = -\partial_x \int_{h_1}^{h_2} u_2 \,\mathrm{d}z, \tag{3.3}$$

and obtain

$$\partial_t h_1 = \frac{1}{\mu}\partial_x \left[\left(\frac{h_1^3}{3} + b\, h_1^2 \right) \partial_x p_1 + \left(\frac{h_1^2}{2} h + b\, h_1 h \right) \partial_x p_2 \right], \tag{3.4a}$$

$$\partial_t h = \partial_x \left[\left(\frac{1}{3} h^3 + \frac{1}{\mu} h_1 h^2 + \frac{b}{\mu} h^2 + \frac{\mu+1}{\mu}\, b_1\, h^2 \right) \partial_x p_2 + \left(\frac{1}{\mu} \frac{h_1^2}{2} h + \frac{b}{\mu} h_1 h \right) \partial_x p_1 \right], \tag{3.4b}$$

where

$$\partial_x p_1 = -\,(\sigma+1)\,\partial_x \left(\partial_{xx} h_1 + \frac{1}{\sigma+1} \partial_{xx} h \right), \tag{3.4c}$$

$$\partial_x p_2 = -\partial_x \left(\frac{\sigma}{\sigma+1} \partial_{xx} h - \phi'(h) \right) + \frac{1}{\sigma+1} \partial_x p_1. \tag{3.4d}$$

This can be written as

$$\partial_t \mathbf{h} = \partial_x \left(Q \cdot \partial_x \mathbf{p} \right), \tag{3.5a}$$

where $\mathbf{h}$ denotes the vector $(h_1(x,t), h(x,t))$, $\mathbf{p} = (p_1(x,t), p_2(x,t))$, and Q the mobility matrix given by

$$Q = \frac{1}{\mu} \begin{pmatrix} \frac{h_1^3}{3} + b\, h_1^2 & \frac{h_1^2 h}{2} + b\, h_1 h \\ \frac{h_1^2 h}{2} + b\, h_1 h & \frac{\mu}{3} h^3 + h_1 h^2 + b\, h^2 + (\mu+1)\, b_1 h^2 \end{pmatrix}. \tag{3.5b}$$

Note also that (3.4c) and (3.4d) are equivalent to

$$\partial_x p_2 = -\partial_x (\partial_{xx} h_2 - \phi'(h)), \tag{3.6a}$$

$$\partial_x p_1 = -\partial_x (\sigma\, \partial_{xx} h_1 + \phi'(h)) + \partial_x p_2 = -\partial_x (\sigma\, \partial_{xx} h_1 + \partial_{xx} h_2). \tag{3.6b}$$

3.2 Strong-slip model

We now assume that during the dewetting motion of the upper from the lower layer there is significant slip at both the solid substrate and the liquid–liquid interface. The systematic derivation of one-layer thin-film models for different regimes of slip at the substrate [21] has shown that the case of strong slip, where the dimensionless slip length is $O(\varepsilon_\ell^{-2})$, represents a distinguished limit. It leads to a particularly rich model that incorporates the effect of elongational stresses. We therefore consider strong slip at both $z = 0$ and $z = h_1$ and introduce slip parameters of $O(\varepsilon_\ell^{-2})$ at the bottom and liquid–liquid interface, respectively,

$$b = \frac{\beta}{\varepsilon_\ell^2}, \quad b_1 = \frac{\beta_1}{\varepsilon_\ell^2}. \tag{3.7}$$

Also, guided by the derivation [21], the plug-flow scaling in both layers leads to $\mathrm{Ca} = \varepsilon_\ell$, and thus here $\alpha = \varepsilon_\ell$. Expanding all dependent variables in terms of ε_ℓ^2, we find that, to leading order, the lateral velocity fields u_i turn out to be constant in z, i.e. we have plug flow in both layers. To obtain closed-form thin-film models for h, h_1 and the lateral velocities u_1 and u_2, the derivation needs to consider the problem to order $O(\varepsilon_\ell^2)$ to obtain solvability conditions. The resulting velocity fields and the leading-order film profiles $h_1(x,t)$ and $h(x,t)$ satisfy the following system of equations:

$$0 = -\partial_x(-(\sigma+1)\partial_{xx} h_1 - \partial_{xx} h) + \frac{4\mu}{h_1} \partial_x(\partial_x u_1 h_1) + \frac{\mu(u_2 - u_1)}{(\mu+1)\beta_1 h_1} - \frac{\mu\, u_1}{\beta h_1}, \tag{3.8a}$$

$$\partial_t h_1 = -\partial_x (h_1 u_1), \tag{3.8b}$$

$$0 = -\partial_x(\phi'(h) - \partial_{xx} h_1 - \partial_{xx} h) + \frac{4}{h} \partial_x(\partial_x u_2 h) - \frac{\mu(u_2 - u_1)}{(\mu+1)\beta_1 h}, \tag{3.8c}$$

$$\partial_t h = -\partial_x (h u_2). \tag{3.8d}$$

We avoid interruption of the flow of argument and include the details of the derivation of this new model in Appendix 1.

4 Linear stability

4.1 Dispersion relation for weak-slip model

We investigate the stability of the stationary solution with two flat interfaces. Since we have assumed in the non-dimensionalisation (2.8) that the length scale H is the typical thickness of the top liquid layer, the base state is given by

$$h_1(x,t) = h_1^0, \qquad h(x,t) = 1.$$

We introduce normal mode perturbations according to

$$h_1(x,t) = h_1^0 + \delta\chi_1 \exp(\mathrm{i}kx + \omega t), \qquad h(x,t) = 1 + \delta(\chi_2 - \chi_1)\exp(\mathrm{i}kx + \omega t),$$

where $\mathrm{i} = \sqrt{-1}$ is the imaginary unit, k the wavenumber and ω the growth rate of the normal mode perturbation, respectively, and $0 < \delta \ll 1$. The notation is chosen to be consistent with expansions where perturbations $\delta\chi_1 \exp(\mathrm{i}kx + \omega t)$ and $\delta\chi_2 \exp(\mathrm{i}kx + \omega t)$ are applied to h_1 and h_2, respectively. We assume that χ_1 and χ_2 are normalised so that $\chi_1^2 + \chi_2^2 = 1$. Substituting this into (3.4a) after eliminating p_1 and p_2, expanding to first order in terms of δ, and dropping the superscript '0', we obtain the following eigenvalue problem for the eigenvalue ω and the eigenvector $\bar{\boldsymbol{\chi}} = (\chi_1, \chi_2 - \chi_1)$:

$$\omega\bar{\boldsymbol{\chi}} = -k^2 QE\bar{\boldsymbol{\chi}}, \tag{4.1}$$

where Q is the mobility matrix (3.5b) with $h = 1$ and

$$E = \begin{pmatrix} (\sigma+1)k^2 & k^2 \\ k^2 & k^2 + \phi''(1) \end{pmatrix}. \tag{4.2}$$

Therefore, the dispersion relation is given by

$$\omega_{1,2} = -\frac{k^2}{2}\mathrm{Tr}(QE) \pm k^2\sqrt{\frac{\mathrm{Tr}(QE)^2}{4} - \mathrm{Det}(QE)}. \tag{4.3}$$

For each value of k, there are two eigenvalues. For positive h_1, b, μ and σ, these are always real and then have a different sign if $\det E < 0$. In fact, one eigenvalue is positive (and the other negative) if $k < k_\mathrm{c}$, and both are stable for $k > k_\mathrm{c}$, where the cut-off wavenumber k_c is obtained from the condition $\det E = 0$, with the result

$$k_\mathrm{c} = \left[\frac{\sigma+1}{\sigma}\right]^{1/2}. \tag{4.4}$$

4.1.1 No slip: $b = b_1 = 0$

To provide a baseline for the discussion on the impact of slip on stability, we first investigate how the dispersion relations and the corresponding perturbations of the two interfaces are affected by different thicknesses h_1 of the lower layer in the case where there is no slip at all, $b = b_1 = 0$. As we mentioned in our introduction, such studies have been carried out before, e.g. in [2] or [6], where different long-range and short-range potentials were used, and dependencies of the stability properties on the film thickness of the two layers, their surface tension and viscosity ratios were investigated. Further studies into the non-linear stability regimes were also undertaken in [7] and [3], which is not the focus of the present study when discussing the impact of slip. In our studies we focus on situations where the surface tension of the liquid–liquid interface is lower by an order of magnitude than that of the gas–liquid interface since we believe this reflects many physical situations. We therefore choose a small value for $\sigma = 0.1$. For simplicity, we assume that the two liquids have the same viscosity, i.e. $\mu = 1$. Moreover, the value of $|\phi''(1)|$ can be scaled out of the problem by rescaling $k = |\phi''(1)|^{1/2}\tilde{k}$ and $\omega = |\phi''(1)|^2\tilde{\omega}$; thus, we can set $\phi'' = -1$ without losing generality. With these parameters, $k_\mathrm{c} = 3.32$.

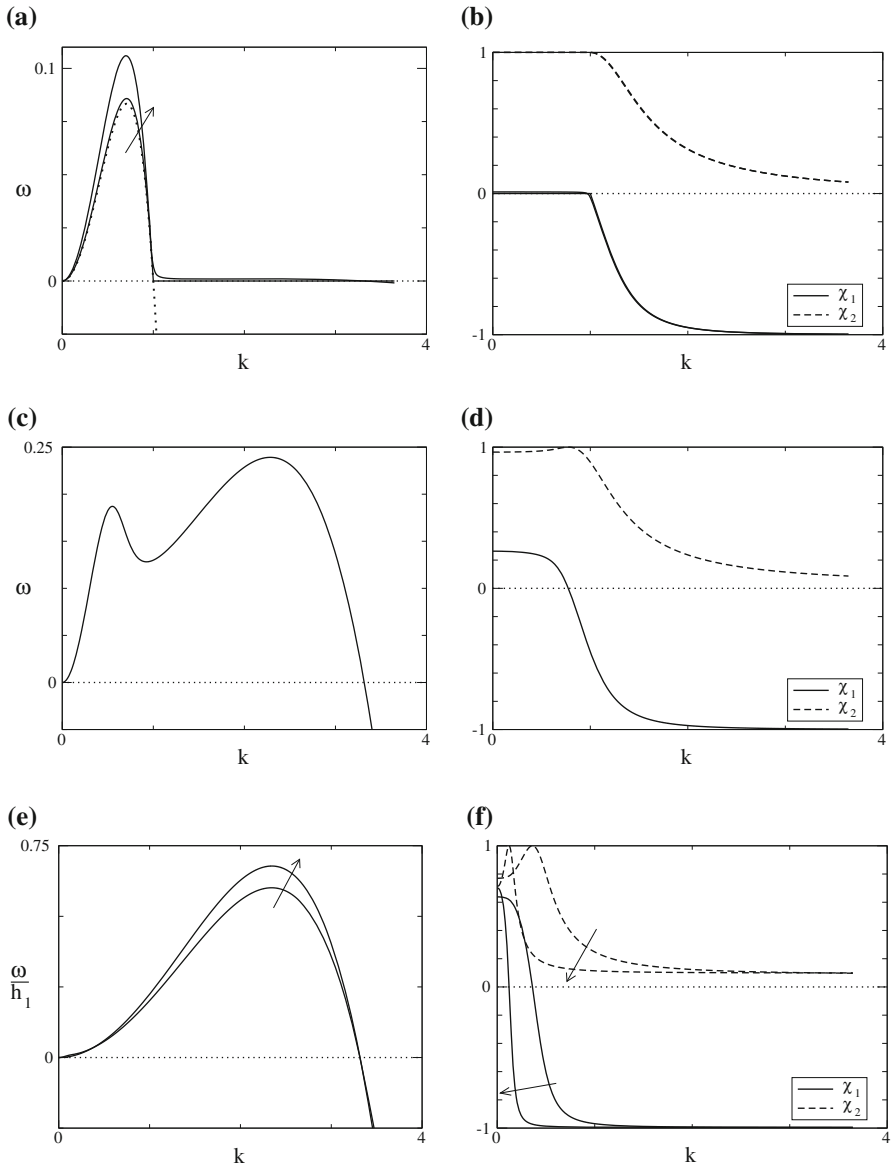

Fig. 2 Dispersion relations (*left column* (**a**, **c**, **e**)) and components of the perturbation vector (*right column* (**b**, **d**, **f**)) for the weak-slip model with $b = b_1 = 0$. The film thickness of the bottom layer is varied from *top to bottom*, with $h_1 = 0.1$, 0.01 in the *top row*, $h_1 = 1$ in the middle and $h_1 = 10$, 100 in the *bottom row*. *Arrows* point in the direction of larger h_1. Values for other parameters are $\mu = 1,\ \sigma = 0.1,\ h = 1$ and $\phi''(1) = -1$. The two components χ_1 and χ_2 of the perturbation vector represent the amplitudes $\delta\chi_1$ and $\delta\chi_2$ of the normal mode perturbations of the lower and upper interfaces, respectively

For moderate thickness of the lower layer ($h_1 = 1$), the most prominent feature to observe are the two maxima in the dispersion relation in Fig. 2c, suggesting a bimodal instability with two different wavelengths. Such a dispersion relation with two maxima was first observed by Pototsky et al. [2] for a situation with three interaction potentials and no slip at both interfaces. Inspection of the components of the perturbation vector $\bar{\chi}$ reveals a transition in the shape of the perturbed layers as k increases from the range where ω has its first maximum to where it has its second maximum. For k less than approximately one, the shape of the perturbation is sinuous-like (both interfaces are perturbed in the same direction), and for k larger than about one it is varicose. However, the modes are quite asymmetric. For the $k \geq 2$, the gas–liquid interface is only weakly perturbed, and in fact the relative amplitude

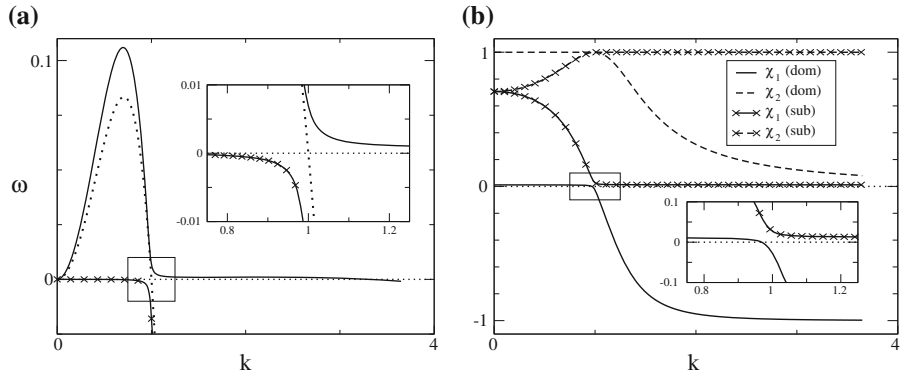

Fig. 3 Dispersion relation (in (**a**)) and components of χ (in (**b**)) for $b = b_1 = 0$, $\mu = 1$, $\sigma = 0.1$, $h = 1$, $h_1 = 0.1$ and $\phi''(1) = -1$ for the dominant and subdominant modes. The values for ω in (**a**) and the values χ_1 and χ_2 in (**b**) for the subdominant mode are emphasised by crosses. (In the legends, 'sub' and 'dom' are abbreviations for 'subdominant' and 'dominant', respectively.) In each *subfigure*, *insets* show zooms of the regions delimited by boxes. As before, the two components χ_1 and χ_2 of the perturbation vector represent the amplitudes $\delta\chi_1$ and $\delta\chi_2$ of the normal mode perturbations of the lower and upper interfaces, respectively

compared to the perturbation of the liquid–liquid interface tends to zero if σ is made smaller. This is plausible since $\sigma \to 0$ implies a very stiff gas–liquid interface, $\sigma_2 \gg \sigma_1$. For longer wavelengths, surface tension should be less important at both interfaces, so that the stability is governed by the intermolecular forces and geometrical constraints, i.e. the presence of a solid substrate below the bottom layer. The latter is expected to have a stronger suppressing effect on the liquid–liquid interface deformation; thus, for $k < 1$ the gas–liquid interface is perturbed more strongly than the liquid–liquid interface.

For small values of the thickness of the lower layer, $h_1 = 0.1$ and $h_1 = 0.01$, we expect the impact of geometric constraints to be more relevant closer to the substrate. Indeed, for k less than approximately one, the sinuous mode in Fig. 2b is more asymmetric than previously in Fig. 2d, with $\chi_2 = O(h_1^2)$, so that in the limit $h_1 \to 0$, only the gas–liquid interface is perturbed. We then have a transition in the relative amplitudes for k between one and two as before. In fact, the relative amplitudes for larger k are similar to those in Fig. 2d. However, if we look at the dispersion relation Fig. 2a, the growth rates for $k > 1$ are small compared to the growth rates for $k < 1$. Thus, the geometric constraints suppress the instability in the range of $k > 1$ and eliminate one of the maxima present for moderate h_1. For $k < 1$, the shape of the perturbation suggest a behaviour as in a one-layer system, and indeed, an asymptotic analysis shows that for $h_1 \ll 1$ one eigenvalue is

$$\omega_{\text{asy}} = -\frac{1}{3}k^2(k^2 - 1) \tag{4.5}$$

to leading order, and the other is zero (i.e. not order one in h_1). Relation (4.5) has its maximum at the wavenumber $k = \sqrt{1/2}$ and its cut-off wavenumber at 1. The top eigenvalue ω_1 approaches ω_{asy} from above for $k < 1$ and the zero eigenvalue, for $k > 1$. It therefore has its maximum near $k = \sqrt{1/2}$ and is nearly zero, but still positive, for $k > 1$ up to k_c, after which it is stable (i.e. negative).

In contrast, the subdominant mode approaches zero from below for $k < 1$ and ω_{asy} for $k > 1$ and is always stable. This is shown for one set of parameter values in Fig. 3a. The two asymptotic approximations of ω, i.e. ω_{asy} and zero, cross at $k = 1$, and this crossing point is approached by the graphs for the subdominant and dominant modes. The minimum distance between the two modes decreases to zero as $h_1 \to 0$ but remains finite for $h_1 > 0$, i.e. they do not cross. Notice also that in Fig. 3b the perturbation amplitude vectors are never identical since the amplitudes χ_2 for the two modes are always separated, although they get close to each other near $k = 1$.

Returning to Fig. 2, we observe that for large $h_1 = 10$ and $h_1 = 100$, the other maximum in the dispersion relation dominates (Fig. 2e). For the wavenumbers where it is located, the shape of the perturbation is that of a varicose mode where the perturbation affects both interfaces in opposite directions. However, due to the smallness of σ, the gas–liquid interface is much stiffer than the liquid–liquid interface; thus the effect of the perturbation

on the former is small. In the long wave regime, the shape of the perturbations is sinuous-like and increasingly symmetric, i.e. it affects both interfaces equally well as $h_1 \to \infty$. The region of k with the sinuous shape in Fig. 2f is thinner than for previously discussed h_1, of order $O(h_1^{-1/2})$. Notice that growth rates in this regime for k are small compared to the maximum rates achieved for $k > 1$.

Summarising, we have for moderate thickness h_1 and small σ, i.e. relatively soft liquid–liquid interface, a bimodal instability. The longer-wave maximum corresponds to a one-layer model where the perturbations occur mainly at the liquid–gas interface while they are inhibited at the liquid–liquid interface due to the constraints from the presence of the substrate. The shorter-wave maximum corresponds to the dominant mode of a one-layer system of thickness $h = 1$ with two interfaces at a distance from any solid substrate. The instability is dominant at the softer, i.e. the liquid–liquid interface. The lower surface tension of this interface determines the preferred wavelength.

4.1.2 General b_1, with $b = 0$

We now investigate how the dispersion relation and perturbation shapes change for moderate, small and large h_1 if b_1 is increased. All other parameter values are retained from the previous numerical experiments. Starting with $h_1 = 1$, in Fig. 4d, we notice that the components of the perturbation vector shown in Fig. 4b change comparatively little. The transition from an asymmetric sinuous to an asymmetric varicose shape at $k = 1 \ldots 2$, already observed for $b_1 = 0$, persists for larger slip. At the upper end of the k shown, the graphs for χ_1 and χ_2 are very similar. The strongest dependence on b_1 is seen for $k < 1$, where $\chi_1 \to 0$ as $b_1 \to \infty$, i.e. the already weak coupling between the interfaces is further diminished.

In the dispersion relation Fig. 4c, increasing b_1 increases ω [notice that for better visibility we plotted ω over $(1 + b_1)$ instead of ω]. This is to be expected since this decreases friction, which accelerates the evolution of the instability. However, the values for ω with k less than approximately one increase like $\propto b_1$ for $b_1 \to \infty$, while the increase of ω for wavenumbers larger than one is smaller. This is not surprising since the lower-k instability mainly involves the gas–liquid interface (as seen in Fig. 4b), for which the friction reduction is stronger than for the liquid–liquid interface, which is more directly affected by the no-slip condition at the solid substrate. The preferential increase of the growth rates allows the lower-k instability to eventually overtake the larger-k instability.

For small $h_1 = 0.1$, we therefore expect that the lower-k instability will be further reinforced. Indeed, the dispersion relation in Fig. 4a does not change qualitatively with increasing b_1, except that the maximum growth rates increase approximately linearly in b_1 for larger slip lengths. The shape of the perturbations are hardly affected by changes in b_1 over two orders of magnitude, as shown in Fig. 4b, where the lines for χ_1 and for χ_2 for the different b_1 nearly coincide.

The effect of increasing b_1 is more dramatic for larger h_1. For $h_1 = 10$ and $b_1 = 0$, the dispersion relation Fig. 4e has only one maximum at k larger than one, with a preferential perturbation of the liquid–liquid interface (Fig. 4f). As b_1 is increased, the lower-k maximum appears again, for the instability that mainly affects the gas–liquid interface. Thus, we recover a bimodal situation. As b_1 is increased even further, the lower-k maximum eventually dominates. Thus we transition from a shorter wavelength perturbation that affects mainly the liquid–liquid interface to a longer wavelength perturbation of predominantly the gas–liquid interface simply by increasing the slip length.

4.2 Dispersion relation for strong-slip thin-film model

We use the same base state and perturbations for the film h_1 and h as in Sect. 3.2. For the velocities u_1 and u_2 the base state is zero, and thus the perturbed field is

$$u_1(x,t) = \delta u_1^1 \exp(\mathrm{i}kx + \omega t), \qquad u_2(x,t) = \delta u_2^1 \exp(\mathrm{i}kx + \omega t).$$

After expanding, the perturbations of the velocity fields can be eliminated, and one obtains the eigenvalue problem

$$\omega \bar{\chi} = k^2 Q_1 T^{-1} Q_2 E \bar{\chi}, \tag{4.6}$$

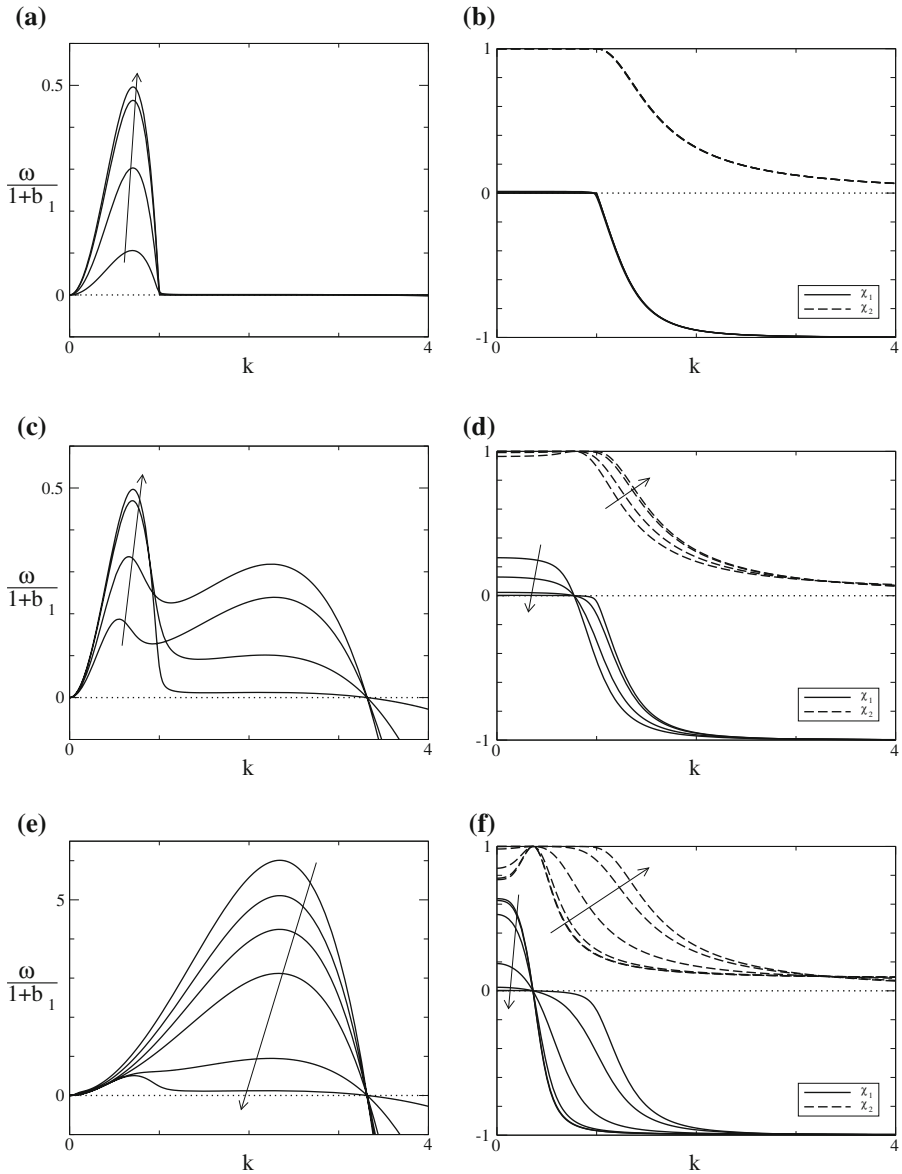

Fig. 4 Dispersion relations (*left column* (**a**, **c**, **e**)) and components of the perturbation vector (*right column* (**b**, **d**, **f**)) for the weak-slip model with $b = 0$ and different slip length $b_1 = 0,\ 1,\ 10,\ 100$ in each panel. The *bottom row* has two additional values, $b_1 = 1{,}000$ and 10^4. All *arrows* point in the direction of increasing b_1. From *top to bottom*, the thickness changes from $h_1 = 0.1$ (*top*) to $h_1 = 1$ (*middle*) and $h_1 = 10$ (*bottom row*). Values for other parameters: $\mu = 1,\ \sigma = 0.1,\ h = 1$ and $\phi''(1) = -1$. Notice that ω was rescaled by $1 + b$ in the *left column*. The two components χ_1 and χ_2 of the perturbation vector represent the amplitudes $\delta\chi_1$ and $\delta\chi_2$ of the normal mode perturbations of the lower and upper interface, respectively

where $\bar{\boldsymbol{\chi}} = (\chi_1, \chi_2 - \chi_1)$, and the matrices are

$$Q_1 = \begin{pmatrix} h_1 & 0 \\ 0 & 1 \end{pmatrix}, \qquad Q_2 = \begin{pmatrix} \beta(\mu+1)\beta_1 h_1 & 0 \\ 0 & (\mu+1)\beta_1 \end{pmatrix}, \qquad E = \begin{pmatrix} (\sigma+1)k^2 & k^2 \\ k^2 & k^2 + \phi''(1) \end{pmatrix}, \tag{4.7}$$

and

$$T = \begin{pmatrix} -4\mu\beta(\mu+1)\beta_1 h_1 k^2 - \mu\beta - \mu(\mu+1)\beta_1 & \mu\beta \\ \mu & -4(\mu+1)\beta_1 k^2 - \mu \end{pmatrix}. \tag{4.8}$$

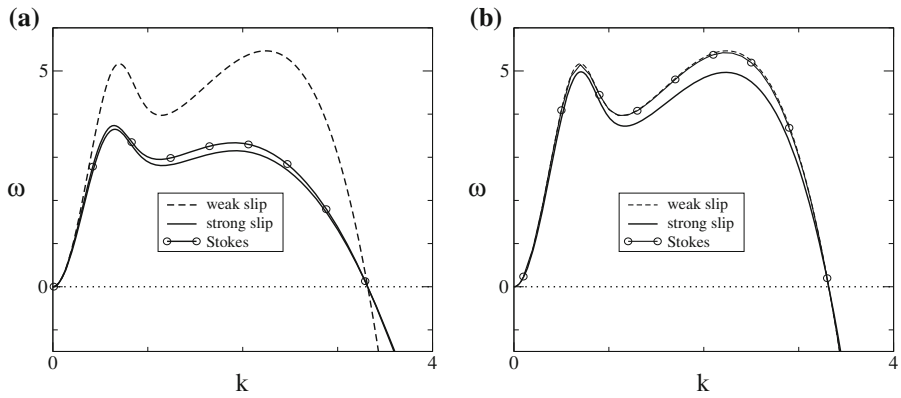

Fig. 5 Comparison between dispersion relations from weak-slip model, strong-slip model and numerical solutions of Stokes equations from Appendix 2. The variables are shown here in the scalings used for the weak-slip model in Sect. 3.1. For the thin-film parameter values, we choose $h_1 = h = 1$, $b = 2$, $b_1 = 10$, $\sigma = 0.1$, $\mu = \mu_1 = \mu_2 = 1$ and $\phi''(h) = -1$. In **a**, we let $\varepsilon_\ell = 0.1$, and $\sigma_1 = 10$ and $\sigma_2 = 100$ for the Stokes model. Also notice this entails $\beta = 0.02$ and $\beta_1 = 0.2$ for the strong-slip model. In **b**, we use $\varepsilon_\ell = 0.01$, $\sigma_1 = 10^3$ and $\sigma_2 = 10^4$, and $\beta = 2 \times 10^{-4}$ and $\beta_1 = 2 \times 10^{-3}$

Therefore, the dispersion relation is given by

$$\omega_{1,2} = -\frac{k^2}{2}\mathrm{Tr}(\bar{Q}E) \pm k^2\sqrt{\frac{\mathrm{Tr}(\bar{Q}E)^2}{4} - \mathrm{Det}(\bar{Q}E)}, \tag{4.9}$$

where $\bar{Q} = -Q_1 T^{-1} Q_2$.

For the parameters, we assume $\mu = 1$ and $\sigma = 0.1$ as before, $h_1 = 10$, and vary β and β_1. As before, the value of $|\phi''(1)|$ can be set to $\phi''(1) = -1$ since by rescaling $k = |\phi''(1)|^{1/2}\tilde{k}$, $\omega = |\phi''(1)|\tilde{\omega}$, $\beta = \tilde{\beta}/|\phi''(1)|$ and $\beta_1 = \tilde{\beta}_1/|\phi''(1)|$, we can remove $\phi''(1)$ from the dispersion relation.

For $\beta_1 = 0.05$, we have, for very small slip parameters at the solid substrate, a bimodal situation. As β is increased, the larger-k maximum dominates, i.e. the instability that mainly affects the liquid–liquid interface in an asymmetric varicose shape. Notice that for the larger β, a very long wavenumber local maximum emerges in the dispersion relation that is associated with an increasingly symmetric sinuous shape of the perturbation.

For $\beta_1 = 0.5$ and $\beta_1 = 5$, the situation is similar, except that for the smallest β shown, the dispersion relation has its global maximum in the lower k range where the perturbation only involves the gas–liquid interface. As β is increased, the larger-k maximum takes over with a perturbation that mainly affects the liquid–liquid interface.

4.3 Discussion and comparison with Stokes model

Stability can also be explored directly by linearising and using normal modes for the full model using the Stokes equations. This leads to a more complicated eigenvalue problem for the growth rate that is derived in Appendix 2, Eqs. (7.8)–(7.17). Numerical solutions of this problem (through a solver for generalised eigenvalue problems) give the growth rate over the entire parameter space, and by taking corresponding limits the dispersion relations for the thin film models in this paper can be recovered.

In Fig. 5a we see the dispersion relations for the three models (weak-slip, strong-slip, Stokes). We assume a lubrication parameter $\varepsilon_\ell = 0.1$. Then, for slip lengths $b = 2$ and $b_1 = 10$ we observe that the weak-slip model overestimates the growth rates in the stable regime compared to the Stokes model. Furthermore, while in the dispersion relation of the weak-slip model the second maximum is the dominant one, in the Stokes case the first maximum is dominant. Recall that this also implies a different prediction for the preferred perturbation shape, with the first maximum corresponding to a sinuous and the second to a varicose mode. On the other hand, the strong-slip model matches the Stokes model quite well for these parameters. However, the picture changes if we decrease

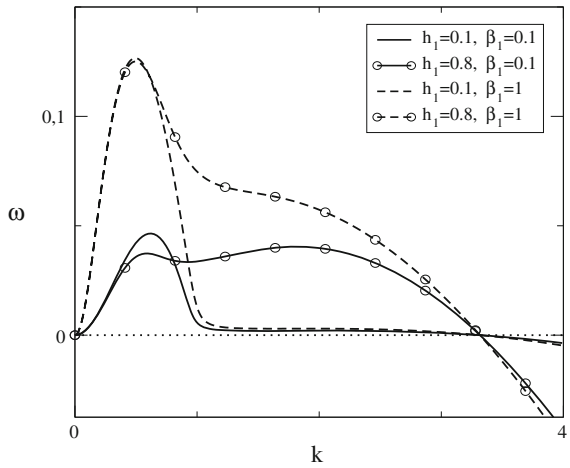

Fig. 6 Effect of varying the thickness of bottom layer for two different values of slip parameter at liquid–liquid interface for strong-slip model. The other slip parameter is $\beta = 0.1$, and the parameters are as before $\mu = 1$, $\sigma = 0.1$, $h = 1$ and $\phi''(1) = -1$

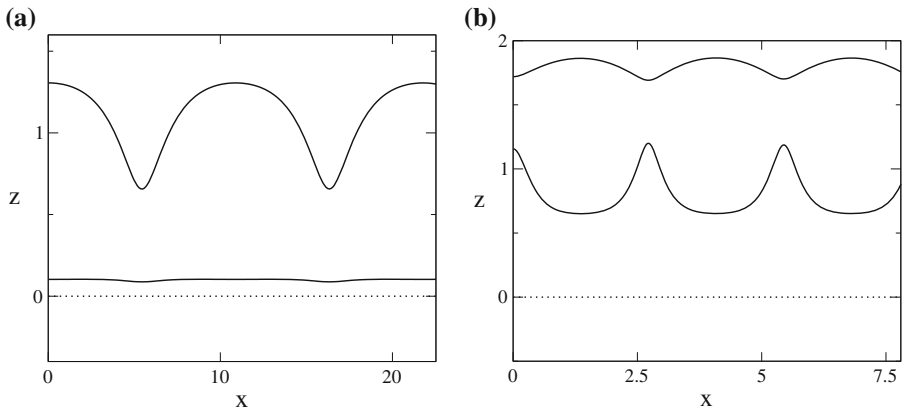

Fig. 7 Numerical simulations of film profiles h_1 and h for strong-slip model with potential $\phi'(h)$ as in (2.10). The initial height of the film is $h_1 = 0.1$, $h = 1$ (*left*) and $h_1 = 0.8$, $h = 1$ (*right*). The parameters are $\beta_1 = \beta = 0.1$, $\mu = 1$ and $\sigma = 0.1$. The profiles were computed using a finite-difference discretisation on a large computational domain with Neumann conditions at the boundary and initial conditions $h_1 = 0.1$, $h = 1 + 0.1\cos(0.577x)$ for (**a**) and $h_1 = 0.8 + 0.1\cos(2.309x)$, $h = 1 - 0.1\cos(2.309x)$ for (**b**)

the lubrication parameter ε_ℓ while keeping the other parameters fixed. Then the weak-slip model gives a better approximation of the Stokes result than the strong-slip model, as we observe in Fig. 5b.

In general, our results show that increasing slip at the liquid–solid interface amplifies perturbations at the liquid–liquid interface relative to the gas–liquid interface, whereas increasing slip at the liquid–liquid interface favours perturbations at the gas–liquid interface.

Also, if the bottom film layer is thick enough, the preferred wavelength perturbation predominantly affects the liquid–liquid interface since the maximum of the dispersion relation corresponds to wavenumbers where χ_1 is larger (Fig. 2e, f). This interface is softer, i.e. easier to deform than the gas–liquid interface, due to its lower surface tension. The preferred wavelength is determined by the smaller surface tension of this interface. If h_1 is decreased, this instability is suppressed. Instead, another maximum of the dispersion relation at smaller wavenumbers appears and eventually becomes dominant (Fig. 2a). The case of moderate film thickness h_1 in Fig. 2c shows both maxima simultaneously. This trend observed for no slip at the solid–liquid and liquid–liquid interface persists for weak slip at the liquid–liquid interface and also for strong slip at both interfaces. Increasing slip at the liquid–liquid interface (and no or fixed weak slip at the solid substrate) delays this transition in the dispersion relation from one dominant maximum to the other as the thickness h_1 is increased. This is also illustrated by Fig. 6. For the smaller slip $\beta_1 = 0.1$,

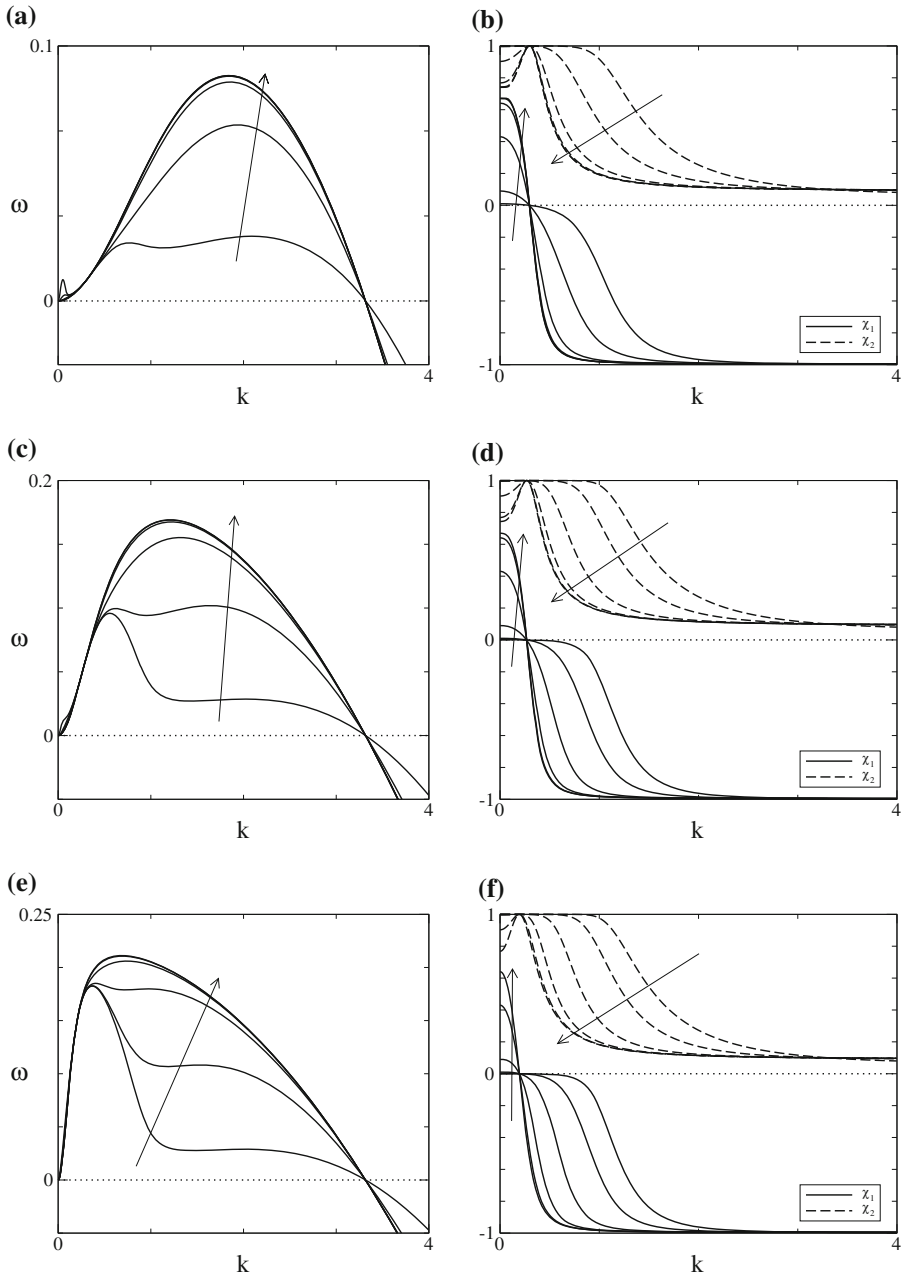

Fig. 8 Dispersion relations (*left column*) and components of the perturbation vector at both interfaces (*right column*) for for the strong-slip model with $h_1 = 10$ and for $\beta_1 = 0.05$, 0.5 and 5, *top to bottom*. Each *subfigure* shows the results for different values of $\beta = 10^{-4}$, 10^{-3}, 0.01, 0.1, 1, 10, with the *arrows* pointing in the direction of increasing β. Values for other parameters are $\mu = 1$, $\sigma = 0.1$, $h = 1$ and $\phi''(1) = -1$. The two components χ_1 and χ_2 of the perturbation vector represent the amplitudes $\delta\chi_1$ and $\delta\chi_2$ of the normal mode perturbations of the lower and upper interface, respectively

the line with $h_1 = 0.8$ has two maxima with the one to the right ($k > 1$) being the larger one. In contrast, for $\beta_1 = 1$, a second maximum is just about to form in the graph for $h_1 = 0.8$ and is clearly dominated by the maximum at $k < 1$. Also in this situation we observe a change in the shape of the preferred wavelength perturbation. While in the case $h_1 = \beta_1 = 0.1$ the perturbation has a sinuous shape (Fig. 7a), the picture changes for the case $h_1 = 0.8$ and $\beta_1 = 0.1$. Here the second maximum becomes dominant and the shape of the perturbation is varicose (Fig. 7b).

In addition, we observed that changing the slip length at the liquid–liquid interface in the weak-slip regime typically does not have a strong effect on the location of the maxima. In contrast, for strong slip at both interfaces, increasing the slip parameter tends to shift the location of the maxima to smaller wavenumbers (cf. Fig. 8a, c, e). We note at this point that for one-layer films with strong slip at the liquid–solid interface, a similar behaviour of the strong-slip and weak-slip thin-film models has been observed previously [20,35].

5 Conclusions and outlook

In this study we derived and compared two thin-film models for liquid–liquid systems accounting for different magnitudes of interfacial slip at their solid–liquid and liquid–liquid interfaces with respect to their interfacial stability properties. One of the thin-film models included weak-slip interface conditions, while the second allowed for strong slip at the interfaces. Stability was also explored directly by linearising and using normal modes for the underlying Stokes equations, which led to an eigenvalue problem for the growth rate, which we numerically solved over the entire parameter space. Taking appropriate limits, the dispersion relations for the two thin-film models in this paper were recovered and, hence, makes it possible to determine the range of validity of the thin-film models when varying slip lengths.

While it had previously been shown that the thickness of liquid layers has an important influence on the stability properties of a liquid–liquid system, our investigations demonstrated that interfacial slip can have a major impact as well.

In conclusion, we note that our results clearly demonstrate that including slip and choosing the appropriate thin-film model is vital for comparisons with experimental data and interpreting, as well as controlling, pattern formation in such systems. The experimental systems we intend to describe with our models typically consist of polymer films such as polystyrene (PS) on top of polymethylmethacrylate (PMMA) with a film thickness of approximately 10–100 nm. As an example, we mention our recent study [36], where we used values for the surface tension $\sigma \approx 0.038$, $\epsilon_\ell = 0.15$ and $\mu = 271$, at a temperature of approximately $T = 140\,^\circ$C for molecular weights of $Mw = 9.6$ kg/mol for PS and $M_\mathrm{w} = 9.9$ kg/mol for PMMA, which have glass transition temperatures of approximately 85 and 115 °C, respectively. While it is already non-trivial to obtain such values, since they are dependent on the temperature and molecular weights of the polymers, obtaining values for the slip length is a matter of future research. It was previously demonstrated in [22,25] for the case of single-layer dewetting polymer films on hydrophobic solid substrates that it is possible to extract quantitative information on the slip parameters from observations of the morphology. The present study has laid down the basic framework for extending this approach to two-layer systems.

A further natural extension of our studies would be to investigate the evolution of the instability beyond the initial linear stages, to consider, for example, the impact of slip on rupture events in a two-layer system. For the no-slip case this has been discussed for example in [2] or [7] and recently also a self-similar approach to rupture was treated in [37]. Extending the work by [38,39], it was shown in [40,41] that the presence of slip introduces a rich structure to a self-similar behaviour. We expect that the two-layer system will exhibit even more complex behaviour due to the additional degrees of freedom arising from the presence of two deformable interfaces.

Acknowledgments The authors SJ, DP and BW are grateful for the support by the DFG of their project within the priority programme SPP 1506, 'Transport at Fluidic Interfaces'.

6 Appendix 1: Derivation of thin-film model for strong slip at liquid–liquid and solid–liquid interfaces

We expand the variables in (2.12) as

$$(u_1, w_1, u_2, w_2) = \left(u_1^{(0)}, w_1^{(0)}, u_2^{(0)}, w_2^{(0)}\right) + \varepsilon_\ell^2 \left(u_1^{(1)}, w_1^{(1)}, u_2^{(1)}, w_2^{(1)}\right) + O\left(\varepsilon_\ell^4\right), \tag{6.1a}$$

$$(p_1, p_2) = \left(p_1^{(0)}, p_2^{(0)}\right) + \varepsilon_\ell^2 \left(p_1^{(1)}, p_2^{(1)}\right) + O\left(\varepsilon_\ell^4\right), \tag{6.1b}$$

$$(h_1, h_2) = \left(h_1^{(0)}, h_2^{(0)}\right) + \varepsilon_\ell^2 \left(h_1^{(1)}, h_2^{(1)}\right) + O\left(\varepsilon_\ell^4\right). \tag{6.1c}$$

and consider in turn the leading- and next-order problem in ε_ℓ.

Leading-order problem

$$0 = \partial_{zz} u_2^{(0)}, \tag{6.2a}$$

$$0 = -\partial_z p_2^{(0)} + \partial_{zz} w_2^{(0)}, \tag{6.2b}$$

$$0 = \partial_x u_2^{(0)} + \partial_z w_2^{(0)}, \tag{6.2c}$$

$$0 = \partial_{zz} u_1^{(0)}, \tag{6.2d}$$

$$0 = -\partial_z p_1^{(0)} + \mu \partial_{zz} w_1^{(0)}, \tag{6.2e}$$

$$0 = \partial_x u_1^{(0)} + \partial_z w_1^{(0)}. \tag{6.2f}$$

For the boundary condition at the free surface $z = h_2^{(0)}$ we get for the normal, tangential and kinematic conditions, respectively,

$$p_2^{(0)} - \phi'(h^{(0)}) + \partial_{xx} h_2^{(0)} - 2\left(\partial_z w_2^{(0)} - \partial_z u_2^{(0)}\, \partial_x h_2^{(0)}\right) = 0, \tag{6.2g}$$

$$\partial_z u_2^{(0)} = 0, \tag{6.2h}$$

$$\partial_t h_2^{(0)} = w_2^{(0)} - u_2^{(0)} \partial_x h_2^{(0)}. \tag{6.2i}$$

For the boundary condition at the free liquid–liquid interface $z = h_1^{(0)}$ we get for the normal, tangential and kinematic conditions, respectively,

$$p_1^{(0)} - p_2^{(0)} + \phi'(h^{(0)}) + \sigma\, \partial_{xx} h_1^{(0)} - 2\left[\left(\mu \partial_z w_1^{(0)} - \partial_z w_2^{(0)}\right) - \left(\mu \partial_z u_1^{(0)} - \partial_z u_2^{(0)}\right) \partial_x h_1^{(0)}\right] = 0, \tag{6.2j}$$

$$\partial_z \left(\mu u_1^{(0)} - u_2^{(0)}\right) = 0, \tag{6.2k}$$

$$\partial_t h_1^{(0)} = w_1^{(0)} - u_1^{(0)} \partial_x h_1^{(0)}. \tag{6.2l}$$

The impermeability condition at $z = h_1^{(0)}$ between the two liquid layers is given by

$$\left(w_2^{(0)} - w_1^{(0)}\right) - \left(u_2^{(0)} - u_1^{(0)}\right) \partial_x h_1^{(0)} = 0. \tag{6.2m}$$

The slip condition at the liquid–liquid interface $z = h_1^{(0)}$ is

$$u_2^{(0)} = \beta_1 \frac{\mu + 1}{\mu} \partial_z u_2^{(0)}. \tag{6.2n}$$

For the boundary conditions at the substrate we assume impermeability and no slip:

$$w_1^{(0)} = 0, \tag{6.2o}$$

$$\partial_z u_1^{(0)} = 0. \tag{6.2p}$$

From (6.2d), (6.2p) and (6.2a), (6.2h) we conclude

$$u_1^{(0)} = u_1^{(0)}(x, t), \tag{6.3a}$$

$$u_2^{(0)} = u_2^{(0)}(x, t), \tag{6.3b}$$

and thus the horizontal velocity components are independent of z. Using this in (6.2f), (6.2o) and (6.2c), (6.2m) we find

$$w_1^{(0)} = -z \partial_x u_1^{(0)}, \tag{6.4a}$$

$$w_2^{(0)} = -\left(z - h_1^{(0)}\right)\partial_x u_2^{(0)} - \partial_x u_1^{(0)} h_1^{(0)} + (u_2^{(0)} - u_1^{(0)})\partial_x h_1^{(0)}. \tag{6.4b}$$

Using (6.2e), (6.2j) and (6.2b), (6.2g) we find

$$p_1^{(0)} + 2\mu\partial_x u_1^{(0)} + \partial_{xx} h_2^{(0)} + \sigma\partial_{xx} h_1^{(0)} = 0, \tag{6.5a}$$

$$p_2^{(0)} - \phi'\left(h^{(0)}\right) + 2\partial_x u_2^{(0)} + \partial_{xx} h_2^{(0)} = 0, \tag{6.5b}$$

hence also independent of z.

Next-order problem

To close the problem to leading order and determine an equation for $u_1^{(0)}$ and $u_2^{(0)}$, we need to consider the problem to next order. We will formulate here only the equations that are required to accomplish the task of fixing these leading-order velocity components.

The next-order upper and lower layer equations in the bulk are

$$0 = -\partial_x p_2^{(0)} + \partial_{xx} u_2^{(0)} + \partial_{zz} u_2^{(1)}, \tag{6.6a}$$

$$0 = -\partial_z p_2^{(1)} + \partial_{xx} w_2^{(0)} + \partial_{zz} w_2^{(1)}, \tag{6.6b}$$

$$0 = \partial_x u_2^{(1)} + \partial_z w_2^{(1)}, \tag{6.6c}$$

$$0 = -\partial_x p_1^{(0)} + \mu\partial_{xx} u_1^{(0)} + \mu\partial_{zz} u_1^{(1)}, \tag{6.6d}$$

$$0 = -\partial_z p_1^{(1)} + \mu\partial_{xx} w_1^{(0)} + \mu\partial_{zz} w_1^{(1)}, \tag{6.6e}$$

$$0 = \partial_x u_1^{(1)} + \partial_z w_1^{(1)}. \tag{6.6f}$$

The next-order tangential stress boundary conditions at liquid–gas interface $z = h_2^{(0)}$ are

$$\partial_z u_2^{(1)} + \partial_x w_2^{(0)} - 4\partial_x u_2^{(0)}\partial_x h_2^{(0)} = 0, \tag{6.6g}$$

$$\partial_z\left(\mu u_1^{(1)} - u_2^{(1)}\right) + \partial_x\left(\mu w_1^{(0)} - w_2^{(0)}\right) - 4\partial_x\left(\mu u_1^{(0)} - u_2^{(0)}\right)\partial_x h_1^{(0)} = 0. \tag{6.6h}$$

At the liquid–liquid interface $z = h_1^{(0)}$ we have

$$u_2^{(0)} - u_1^{(0)} = \beta_1 \frac{\mu}{\mu + 1}\left[\partial_z u_2^{(1)} + \partial_x w_2^{(0)} - 4\partial_x u_2^{(0)}\partial_x h_1^{(0)}\right], \tag{6.6i}$$

and at the solid substrate $z = 0$,

$$u_1^{(0)} = \beta_1 \partial_z u_1^{(1)}. \tag{6.6j}$$

In the preceding equations, we have already made use of the fact that $u_1^{(0)}$ and $u_2^{(0)}$ do not depend on z and dropped all derivatives of these variables with respect to z.

Integrating now (6.6a) and (6.6d), we obtain

$$\partial_z\, u_2^{(1)}\Big|_{h_2^{(0)}} - \partial_z\, u_2^{(1)}\Big|_{h_1^{(0)}} = -h^{(0)}\left(-\partial_x p_2^{(0)} + \partial_{xx} u_2^{(0)}\right), \tag{6.7a}$$

$$\partial_z\, u_1^{(1)}\Big|_{h_2^{(0)}} - \partial_z\, u_1^{(1)}\Big|_{h_1^{(0)}} = -h_1^{(0)}\left(-\partial_x p_1^{(0)} + \mu\partial_{xx} u_1^{(0)}\right). \tag{6.7b}$$

The pressure terms on the right-hand side can be eliminated by using (6.5a) and (6.5b). The terms on the left-hand side can be expressed in terms of the leading-order solutions $u_2^{(0)}$, $u_2^{(0)}$, $h_1^{(0)}$ and $h_2^{(0)}$ by first using (6.6g), (6.6h),

(6.6i) and (6.6j), then eliminating the occurring $w_2^{(0)}$ and $w_1^{(0)}$ via the solutions (6.4a) and (6.4b). This yields Eqs. (3.8a) and (3.8c). The other two equations, (3.8b) and (3.8d), are obtained by integrating (6.2c) and (6.2f) and using the conditions (6.2i), (6.2l), (6.2m), (6.2p).

7 Appendix 2: Dispersion relations for Stokes equations

We start the stability analysis with the Stokes equations

$$0 = -\partial_x p_n + \mu_n \left(\partial_{xx} u_n + \partial_{zz} u_n\right), \tag{7.1a}$$

$$0 = -\partial_z p_n + \mu_n \left(\partial_{xx} w_n + \partial_{zz} w_n\right), \tag{7.1b}$$

$$0 = \partial_x u_n + \partial_z w_n \tag{7.1c}$$

and the boundary conditions from the previous sections. To simplify our problem, we introduce the stream functions Ψ_1 and Ψ_2 with

$$u_n = \frac{\partial \Psi_n}{\partial z}, \quad w_n = -\frac{\partial \Psi_n}{\partial x} \qquad (n = 1, 2). \tag{7.2}$$

Plugging this into the Stokes equations we obtain two biharmonic equations:

$$\partial_x^4 \Psi_n + 2\partial_x^2 \partial_z^2 \Psi_n + \partial_z^4 \Psi_n = 0 \qquad (n = 1, 2). \tag{7.3}$$

Linear stability is carried out by introducing small perturbations

$$\left(\Psi_n,\ h_1 - h_1^0,\ h_2 - h_2^0,\ p_n - p_n^0,\ \phi - \phi_0\right) = \delta \left(\psi_n(z),\ \chi,\ 1,\ \Pi_n(z),\ (1-\chi)\ \phi'\big|_{h^0}\right) \exp(\mathrm{i}kx + \omega t) \tag{7.4}$$

around the base state

$$\Psi_n = 0, \quad h_n = h_n^0, \quad h^0 = h_2^0 - h_1^0, \quad p_n = p_n^0, \quad \phi|_{h^0} = \phi_0, \tag{7.5}$$

where ω and k are the growth coefficient and the wavenumber, and obtain

$$\partial_z^4 \psi_n - 2k^2 \partial_z^2 \psi_n + k^4 \psi_n = 0, \tag{7.6}$$

with the general solutions

$$\psi_n(z) = u_{n1} \exp(kz) + u_{n2} z \exp(kz) + u_{n3} \exp(-kz) + u_{n4} z \exp(-kz), \tag{7.7}$$

where the coefficients are determined using the boundary conditions. First, slip at $z = 0$ leads to

$$(k - b\,k^2)u_{11} + (1 - 2\,b\,k)u_{12} - (k + b\,k^2)u_{13} + (1 + 2\,b\,k)u_{14} = 0, \tag{7.8}$$

while impermeability simply reads

$$u_{11} + u_{13} = 0. \tag{7.9}$$

At the free surface $z = h_2$ the kinematic condition becomes

$$k\mathrm{e}^{kh_2^0} u_{21} + kh_2^0 \mathrm{e}^{kh_2^0} u_{22} + k\mathrm{e}^{-kh_2^0} u_{23} + kh_2^0 \mathrm{e}^{-kh_2^0} u_{24} = \mathrm{i}\omega \tag{7.10}$$

the tangential stress condition

$$k\mathrm{e}^{kh_2^0} u_{21} + (kh_2^0 + 1)\mathrm{e}^{kh_2^0} u_{22} + k\mathrm{e}^{-kh_2^0} u_{23} + (kh_2^0 - 1)\mathrm{e}^{-kh_2^0} u_{24} = 0. \tag{7.11}$$

At the liquid–liquid interface $z = h_1$, the kinematic condition now reads

$$k\mathrm{e}^{kh_1^0} u_{11} + kh_1^0 \mathrm{e}^{kh_1^0} u_{12} + k\mathrm{e}^{-kh_1^0} u_{13} + kh_1^0 \mathrm{e}^{-kh_1^0} u_{14} = \mathrm{i}\chi\omega \tag{7.12}$$

the tangential stress condition

$$\mu_1 [k\mathrm{e}^{kh_1^0} u_{11} + (kh_1^0 + 1)\mathrm{e}^{kh_1^0} u_{12} + k\mathrm{e}^{-kh_1^0} u_{13} + (kh_1^0 - 1)\mathrm{e}^{-kh_1^0} u_{14}]$$

$$-\mu_2[k\mathrm{e}^{kh_1^0}u_{21}+(kh_1^0+1)\mathrm{e}^{kh_1^0}u_{22}+k\mathrm{e}^{-kh_1^0}u_{23}+(kh_1^0-1)\mathrm{e}^{-kh_1^0}u_{24}]=0. \tag{7.13}$$

The impermeability condition is equivalent to

$$k\mathrm{e}^{kh_1^0}u_{21}+kh_1^0\mathrm{e}^{kh_1^0}u_{22}+k\mathrm{e}^{-kh_1^0}u_{23}+kh_1^0\mathrm{e}^{-kh_1^0}u_{24}=\mathrm{i}\chi\omega \tag{7.14}$$

and, finally, the slip condition

$$\begin{aligned}&k\mathrm{e}^{kh_1^0}u_{11}+(kh_1^0+1)\mathrm{e}^{kh_1^0}u_{12}-k\mathrm{e}^{-kh_1^0}u_{13}-(kh_1^0-1)\mathrm{e}^{-kh_1^0}u_{14}\\&+k(2b_*k-1)\mathrm{e}^{kh_1^0}u_{21}+(kh_1^0+1)(2b_*k-1)\mathrm{e}^{kh_1^0}u_{22}\\&+k(2b_*k+1)\mathrm{e}^{-kh_1^0}u_{23}+(kh_1^0-1)(2b_*k+1)\mathrm{e}^{-kh_1^0}u_{24}=0,\end{aligned} \tag{7.15}$$

where $b_*=(1+\mu_2/\mu_1)b_1$. For the solution of this algebraic system we use the remaining boundary conditions, namely the normal stress conditions at $z=h_2$

$$\mathrm{i}\mu_2[2k^2\mathrm{e}^{kh_2^0}u_{21}+2k^2h_2^0\mathrm{e}^{kh_2^0}u_{22}-2k^2\mathrm{e}^{-kh_2^0}u_{23}-2k^2h_2^0\mathrm{e}^{-kh_2^0}u_{24}]=\sigma_2k^2+(1-\chi)\,\phi''\big|_{h^0}\,, \tag{7.16}$$

and at $z=h_1$

$$\begin{aligned}&\mathrm{i}\mu_1[2k^2\mathrm{e}^{kh_1^0}u_{11}+2k^2h_1^0\mathrm{e}^{kh_1^0}u_{12}-2k^2\mathrm{e}^{-kh_1^0}u_{13}-2k^2h_1^0\mathrm{e}^{-kh_1^0}u_{14}]\\&-\mathrm{i}\mu_2[2k^2\mathrm{e}^{kh_1^0}u_{21}+2k^2h_1^0\mathrm{e}^{kh_1^0}u_{22}-2k^2\mathrm{e}^{-kh_1^0}u_{23}-2k^2h_1^0\mathrm{e}^{-kh_1^0}u_{24}]=\sigma_1\chi k^2-(1-\chi)\,\phi''\big|_{h^0}\,.\end{aligned} \tag{7.17}$$

References

1. Brochard Wyart F, Martin P, Redon C (1993) Liquid/liquid dewetting. Langmuir 9:3682–3690
2. Pototsky A, Bestehorn M, Merkt D, Thiele U (2004) Alternative pathways of dewetting for a thin liquid two-layer film. Phys Rev E 70(2):25201
3. Pototsky A, Bestehorn M, Merkt D, Thiele U (2005) Morphology changes in the evolution of liquid two-layer films. J Chem Phys 122:224711
4. Fisher L, Golovin A (2005) Nonlinear stability analysis of a two-layer thin liquid film: dewetting and autophobic behavior. J Colloid Interface Sci 291:515–528
5. Fisher L, Golovin A (2007) Instability of a two-layer thin liquid film with surfactants: dewetting waves. J Colloid Interface Sci 307:203–214
6. Bandyopadhyay D, Gulabani R, Sharma A (2005) Instability and dynamics of thin liquid bilayers. Ind Eng Chem Res 44:1259–1272
7. Bandyopadhyay D, Sharma A (2006) Nonlinear instabilities and pathways of rupture in thin liquid bilayers. J Chem Phys 125:054711
8. Craster RV, Matar O (2006) On the dynamics of liquid lenses. J Colloid Interface Sci 303:503–506
9. Lenz RD, Kumar S (2007) Competitive displacement of thin liquid films on chemically patterned substrates. J Fluid Mech 571:33–57
10. Lenz RD, Kumar S (2007) Instability of confined thin liquid film trilayers. J Colloid Interface Sci 316:660–670
11. Thiele U, Archer AJ, Plapp M (2012) Thermodynamically consistent description of the hydrodynamics of free surfaces covered by insoluble surfactants of high concentration. Phys Fluids 24:102107
12. Craster RV, Matar O (2009) Dynamics and stability of thin liquid films. Rev Mod Phys 81:1131–1198
13. Lin CC (1979) A mathematical model for viscosity in capillary extrusion of two-component polyblends. Polym J (Tokyo) 11:185–192
14. Zhao R, Macosko C (2002) Slip at polymer–polymer interfaces: rheological measurements on coextruded multilayers. J Rheol 46:145–167
15. Zeng H, Tian Y, Zhao B, Tirrell M, Israelachvili J (2009) Friction at the liquid/liquid interface of two immiscible polymer films. Langmuir 124–132
16. Lin Z, Kerle T, Russell T, Schaffer E, Steiner U (2002) Electric field induced dewetting at polymer/polymer interfaces. Macromolecules 35:6255–6262
17. Brochard-Wyart F, de Gennes P (1992) Shear-dependent slippage at a polymer/solid interface. Langmuir 8:3033–3037
18. Léger L (2003) Friction mechanisms and interfacial slip at fluid–solid interfaces. J Phys Condens Matter 15:S19–S29
19. Lauga E, Brenner MP, Stone H (2007) Microfluidics: the no-slip boundary condition. In: Tropea C, Yarin A, Foss JF (eds) Handbook of experimental fluid dynamics. Springer, New York, pp 1219–1240
20. Kargupta K, Sharma A, Khanna R (2004) Instability, dynamics and morphology of thin slipping films. Langmuir 20:244–253
21. Münch A, Wagner B, Witelski TP (2006) Lubrication models with small to large slip lengths. J Eng Math 53:359–383
22. Fetzer R, Jacobs K, Münch A, Wagner B, Witelski TP (2005) New slip regimes and the shape of dewetting thin liquid films. Phys Rev Lett 95:127801

23. Blossey R, Münch A, Rauscher M, Wagner B (2006) Slip vs viscoelasticity in dewetting thin films. EPhJ E Soft Matter 20:267–271
24. Vilmin T, Raphael E (2005) Dewetting of thin viscoelastic polymer films on slippery substrates. Europhys Lett 72:781
25. Fetzer R, Münch A, Wagner B, Rauscher M, Jacobs K (2007) Quantifying hydrodynamic slip: a comprehensive analysis of dewetting profiles. Langmuir 23:10559–10566
26. Bäumchen O, Fetzer R, Jacobs K (2009) Reduced interfacial entanglement density affects the boundary conditions of polymer flow. Phys Rev Lett 103:247801
27. Goveas J, Fredrickson G (1998) Apparent slip at a polymer–polymer interface. Eur Phys J B Condens Matter Complex Syst 2:79–92
28. Adhikari NP, Goveas JL (2004) Effects of slip on the viscosity of polymer melts. J Polym Sci B Polym Phys 42:1888–1904
29. Brochard-Wyart F, de Gennes P (1993) Sliding molecules at a polymer/polymer interface. C R Acad Sci Ser II(327):13–17
30. Ajdari A (1993) Slippage at a polymer/polymer interface: entanglements and associated friction. C R Acad Sci Ser II 317:1159–1163
31. Ajdari A, Wyart FB, de Gennes PG, Leibler L, Viovy J, Rubinstein M (1994) Slippage of an entangled polymer melt on a grafted surface. Physica A 204:17–39
32. Israelachvili JN (1992) Intermolecular and surface forces. Academic, London
33. Sharma A (1993) Relationship of thin-film stability and morphology to macroscopic parameters of wetting in the apolar and polar sytems. Langmuir 9:861–869
34. Bonn D, Eggers J, Indekeu J, Meunier J, Rolley E (2011) Wetting and spreading. Rev Mod Phys 81:739–805
35. Rauscher M, Blossey R, Münch A, Wagner B (2008) Spinodal dewetting of thin films with large interfacial slip: implications from the dispersion relation. Langmuir 24:12290–12294
36. Bommer S, Jachalski S, Peschka D, Seemann R, Wagner N (2013) Droplets on liquids and their long way into equilibrium. arXiv, preprint arXiv:1212.1183
37. Ward MH (2011) Interfacial thin films rupture and self-similarity. Phys Fluids 23:062105–062105-14
38. Witelski TP, Bernoff AJ (1999) Stability of self-similar solutions for Van der Waals driven thin film rupture. Phys Fluids 11:2443–2445
39. Renardy M (2001) Finite time breakup of viscous filaments. Z Angew Math Phys 52:881–887
40. Peschka D, Münch A, Niethammer B (2010) Thin-film rupture for large slip. J Eng Math 66:33–51
41. Peschka D, Niethammer B, Münch A (2010) Self-similar rupture of viscous thin films in the strong-slip regime. Nonlinearity 23:409–427